Chapter

The Use of Computational Fluid Dynamics in the Analysis of Gas-Liquid-Liquid Reactors

Godfrey Kabungo Gakingo and Tobias Muller Louw

Abstract

Gas–liquid–liquid reactors are typically found in bioprocess setups such as those used in alkane biocatalysis and biological gas stripping. The departure of such reactors from traditional gas–liquid setups is by the introduction of a secondary (dispersed) liquid phase. The introduction of the latter results in complicated hydrodynamics as observed through measurements of velocity fields, turbulence levels and mixing times. Similarly, changes in mass transfer occur as observed through measurements of gas hold up, bubble diameters and the volumetric mass transfer coefficients. The design and analysis of such reactors thus requires the adoption of an approach that can comprehensively account for the various observed changes. This chapter proposes Computational Fluid Dynamics as an approach fit for this purpose. Key considerations, successes and challenges of this approach are highlighted and discussed based on a review of previously published case studies.

Keywords: Gas–liquid–liquid reactors, stirred tanks, hydrodynamics, mass transfer, Computational Fluid Dynamics, predictive modelling

1. Introduction

Multiphase systems comprising of more than two phases are a common occurrence in the fields of chemical and bioprocess engineering. Such multiphase systems may be comprised of a gas phase, a liquid phase and a solid phase as is the case in froth flotation processes in the minerals sector [1, 2]. Alternatively, such multiphase systems may be comprised of a gas phase and two immiscible liquid phases as is often found in biological gas stripping [3] or biocatalysis [4]. Irrespective of the application field, a common expectation among such multiphase systems is that they are characterised by more complex hydrodynamics than two phase systems which are reasonably well understood [5, 6]. Similarly, mixing and mass transfer effects are expected to be more complex in such systems.

Given the above considerations, the design and analysis of multiphase systems requires the use of comprehensive frameworks that are capable of taking into account the various mechanisms of action that are at play. Computational Fluid Dynamics (CFD) has been proposed as one such framework since it is able to describe the hydrodynamics of multiphase systems based on fundamental equations of flows [7]. Furthermore, coupling of CFD simulations to sub-models of mass transfer, mixing or flotation can enable the description of these effects at finer

resolutions than can be obtained based on empirical modelling. Thus, significant effort has been recently directed towards the development and application of CFD techniques to simulate multiphase systems comprising of two phase reactors [8–10] as well as those with more than two phases [2, 11–13].

This chapter builds upon recent work by presenting a discussion on the use of CFD in the design and analysis of gas–liquid–liquid reactors within the context of mass transfer. Key considerations informing the modelling approach have been discussed with their implementation illustrated by the review of recently modelled case studies [12, 13]. Furthermore, the successes and challenges attending the CFD-based modelling of gas–liquid–liquid reactors have been highlighted and on the basis of these, recommendations have been given on areas requiring further investigation. The chapter thus addresses itself to graduate students, academics and industrial practitioners interested in a comprehensive modelling framework for the design and analysis of gas–liquid–liquid reactors.

2. Considerations in gas–liquid–liquid systems

Gas–liquid–liquid reactors are a common occurrence in the bioprocess field (see **Table 1**). Such reactors tend to be comprised of one continuous liquid phase (primary liquid phase) and two dispersed phases (gas phase and secondary liquid phase) as illustrated in **Figure 1**. The departure of such reactors from traditional gas–liquid reactors is through the introduction of a secondary liquid phase within

Primary liquid phase	Secondary liquid phase (volume fraction)	Gas phase	Reactor type (objective)	Reference
Water	n-$C_{11–18}$ alkane cut (0–100%)	Pure oxygen	STR[1] (oxygen transfer)	[14]
	Oleic acid (0–100%)	Pure argon	STR (argon mass transfer)	
Water	n-$C_{12–13}$ alkane cut (0–20%)	Air	STR (oxygen transfer)	[15]
Water	n-Dodecane (0–100%)	Pure oxygen	STR (oxygen transfer)	[16]
	n-Heptane (0–100%)			
	n-Hexadecane (0–100%)			
Water	Silicone oil (0–10%)	Air	BCR[2] (oxygen transfer)	[17]
		Air dosed with styrene	BCR (biological gas stripping[3])	
Water	Anisole (0–10%)	Air	BCR (oxygen transfer)	[18]
	2-ethyl-1-hexanol (0–10%)			
	Decyl alcohol (0–10%)			
	Toluene (0–10%)			
	n-Heptane (0–10%)			
	n-Decane (0–10%)			
	Dodecane (0–10%)			

[1]*STR – stirred tank reactor.*
[2]*BCR – bubble column reactor.*
[3]*For more on biological gas stripping, see [3].*

Table 1.
Selection of experimental work on gas–liquid–liquid reactors.

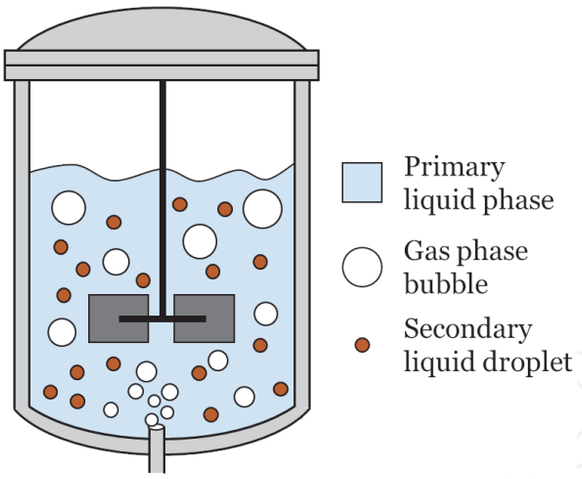

Figure 1.
Illustration of gas–liquid–liquid stirred tank reactor.

the system. The introduction of the latter modifies the system in a manner that impacts mass transfer and this can be seen by changes in the gas hold up, the bubble diameters and the overall volumetric mass transfer coefficients [4]. Underpinning these observable changes, however, are modifications to the fluid properties, mass transfer properties and pathways as well as the reactor hydrodynamics. A consideration of these modifications is necessary for appropriate modelling and as such a brief review on the same is presented herein. In-depth reviews are available elsewhere [4, 19, 20].

2.1 Changes in fluid properties

The introduction of a secondary liquid phase into a traditional gas–liquid reactor can result in a change of fluid properties. For example, the surface tension between the primary liquid phase and the gas phase can change depending on the degree of solubility of the secondary liquid phase in the primary liquid phase. To characterise this, surface tension values based on mutually saturated liquids have been reported in literature [16, 18]. Such values have generally been obtained by mixing the primary liquid phase with the additional liquid phases for long periods followed by a separation of the phases and surface tension measurements using a tensiometer [18]. **Table 2** illustrates selected results from literature.

The results in **Table 2** generally point to a decrease in the saturated surface tension (σ_{sat}) with addition of the secondary liquid phase. Furthermore, this change in surface tension has been observed to be greater when the secondary liquid phase is more soluble in the primary liquid phase [18]. As a decrease in the surface tension results in smaller gas bubbles, an enhancement in mass transfer can be expected. However, this is not always the case. For example, Kundu et al. [18] observed a negative impact on mass transfer upon the addition of toluene, anisole, decyl alcohol and 2-ethyl-1-hexanol despite a decrease in σ_{sat} (refer to **Table 2**). This points to the presence of additional factors that need to be taken into account for a proper description of mass transfer in such systems.

Two additional points need to be highlighted with regard to surface tension. First, discrepancies in the reported values of σ_{sat} exist as seen in **Table 2**. For example, Ngo & Schumpe [16] measured an insignificant change in σ_{sat} (71.8 mN/m) upon the addition of n-Heptane whereas Kundu et al. [18] measured a significant change (σ_{sat} = 65 mN/m). Such discrepancies point to a need for additional experimental measurements of σ_{sat}.

Primary liquid phase	Secondary liquid phase	Saturated surface tension, σ_{sat} (mN/m)	Reference
Water	—	72.8	[18]
	Dodecane	71	
	n-Decane	67	
	n-Heptane	65	
	Anisole	65	
	Toulene	44	
	2-ethyl-1-hexanol	43	
	Decyl-alcohol	38	
Water	—	72	[16]
	n-Heptane	71.8	
	n-Dodecane	68.2	
	n-Hexadecane	71.2	
Deionised water	—	71.69 ±0.14	Author's laboratory
	n-C_{14}-C_{20} alkane cut	60.85 ± 0.50	

Table 2.
Saturated surface tension for various liquid–liquid combinations.

A second point to note is that researchers have also attempted to report on dynamic values of the surface tension [21]. This was achieved by preparation of a "stable" liquid–liquid dispersion followed by measurement of the surface tension [21]. The values obtained were in the range of 17–26 mN/m for an n-C_{10}-C_{13} alkane cut mixed with water [21]. These values were lower than those reported in **Table 2** and tended towards the surface tension values of pure alkanes (23.9 mN/m for n-Decane, 25.41 mN/m for n-Dodecane [18]). Consequently, it may be suggested that a degree of separation of the liquid–liquid dispersion occurred during surface tension measurements despite the best efforts of the researchers. In this case, the settled-out and less dense alkane phase would form an intervening layer between the gas phase and the dispersion.

Besides the above changes to the surface tension, the presence of a secondary liquid phase can lead to changes in *effective* fluid properties such as the effective density, the effective viscosity as well as the effective solubility. The pre-qualifying term, "*effective*", is used in this case since such properties are defined based on a view of the liquid–liquid dispersion as a single pseudo-homogenous liquid. This view permits for a simplification of the 3-phase gas–liquid–liquid reactor to an effective 2-phase reactor. Consequently, correlations derived for traditional 2-phase reactors, such as Eq. (1) with an empirical basis and Eq. (2) with a theoretical basis [5], can be used as a starting point for the design of 3-phase reactors. In these equations, $K_L a$ represents the overall volumetric mass transfer coefficients in a 2-phase reactor whereas x_g and d_g respectively represent the gas hold up and the bubble diameters (see Eq. (3) and (4)). Other variables are as defined in the Nomenclature.

$$K_L a = \Gamma \cdot \left(\frac{P_g}{V}\right)^x \nu_s{}^y \tag{1}$$

$$K_L a = \Lambda \cdot \sqrt{D_c}\left(\frac{P_g/V}{\mu_c}\right)^{0.25} \cdot \left(\frac{6x_g}{d_g}\right) \tag{2}$$

$$d_g = 0.7\left(\frac{\sigma_{gc}^{0.6}}{\rho_c{}^{0.2}\left(\frac{P_g}{V}\right)^{0.4}}\right)\left(\frac{\mu_c}{\mu_g}\right)^{0.1} \tag{3}$$

$$\frac{x_g}{1-x_g} = 0.819\frac{\nu_s{}^{0.67}N^{0.4}T^{0.267}}{g^{0.33}}\left(\frac{\rho_c}{\sigma}\right)^{0.2}\left(\frac{\rho_c}{\rho_c-\rho_g}\right)\left(\frac{\rho_c}{\rho_g}\right)^{-0.067} \tag{4}$$

Effective fluid properties can be specified on the basis of simple mixing rules such as Eq. (5) for the effective density (ρ_{eff}). Such equations consider the contributions of the individual liquid phases based on their volumetric proportions (x_i) but neglect non-ideal effects that may arise from molecular interactions, commonly found in homogeneous mixtures, which may lead to excess volumes. This notwithstanding, experimental evidence suggests that such equations are sufficient for the effective density [22] and the effective solubility (see next section). This may be due to the poor mutual solubility of liquid phases typically tested for gas–liquid–liquid reactor applications: the properties of the individual liquid phases remain unchanged by the presence of a second, immiscible phase and the bulk properties can be estimated by simple volume averaging.

$$\rho_{\text{eff}} = \sum_{i=1}^{n} x_i\rho_i \tag{5}$$

With regard to effective viscosity (μ_{eff}), models of a more complicated form than that given in Eq. (5) are required. This is due to the need to account for the perturbation of fluid flow in the presence of droplets of the secondary liquid phase. Models varying in complexity have been proposed. For example, the Taylor model (see Eq. (6)) has been proposed for dilute dispersions of spherical droplets [23]. Additionally, models such as those given in Eq. (7) and (8) have been proposed for non-dilute dispersions where the hydrodynamic interactions among droplets need to be accounted for [23, 24]. Besides these, however, models have also been proposed to account for non-zero shear rates in the fluid which introduce effects such as droplet deformation [23, 25].

$$\frac{\mu_{eff}}{\mu_c} = 1 + 2.5x_d\left[\frac{0.4+\mu_r}{1+\mu_r}\right]; x_d \to 0 \tag{6}$$

$$\frac{\mu_{eff}}{\mu_c}\left[\frac{2\frac{\mu_{eff}}{\mu_c}+5\mu_r}{2+5\mu_r}\right]^{1.5} = \exp\left(\frac{2.5x_d}{1-x_d/x_m}\right) \tag{7}$$

$$\frac{\mu_{eff}}{\mu_c}\left[\frac{2\frac{\mu_{eff}}{\mu_c}+5\mu_r}{2+5\mu_r}\right]^{1.5} = \left(1-\frac{x_d}{x_m}\right)^{-2.5x_m} \tag{8}$$

In the equations above, μ_r refers to the ratio of viscosity of the secondary liquid phase (μ_d) to that of the primary liquid phase (μ_c). Variables x_d and x_m, on the other hand, refer to the volume fraction of the secondary liquid phase and the maximum packing limit of its droplets respectively.

2.2 Changes in mass transfer properties and pathways

Properties of interest affecting mass transfer include the solubility and diffusivity of a species within the liquid–liquid dispersion. Taking the liquid–liquid dispersion as a pseudo-homogenous liquid, effective properties have been defined. For example, it has been observed that the effective solubility of a species (C^*_{eff}) can be specified according to the volumetric proportions of the liquids involved, once again recognising that the presence of immiscible phases has a negligible effect on the solubilities associated with individual phases [22, 26]. This is illustrated in Eq. (9) below, with C^*_i representing the solubility in liquid phase i and n representing the total number of liquid phases.

$$C^*_{eff} = \sum_{i=1}^{n} x_i C^*_i \tag{9}$$

Given the application fields of gas–liquid–liquid reactors (such as biological gas stripping), the effective solubility is usually higher than the solubility of a species in the primary liquid phase ($C^*_{eff} > C^*_c$). This implies that a longer duration is required to saturate the liquid–liquid dispersion with a given species in comparison to the time required to saturate the pure primary liquid phase [27, 28]. Consequently, for a fixed mass transfer rate, lower values of the overall volumetric mass transfer coefficients can be obtained upon the addition of a secondary liquid phase [28, 29].

With regard to the molecular diffusion of a species, the effective diffusivity (D_{eff}) has been defined as illustrated in Eq. (10) for dilute liquid–liquid dispersions [30]. This equation, being of a general nature, has also been used to describe the effective diffusivity of solid–liquid suspensions [31]. The variable D_r in this equation represents the diffusivity ratio whereas D_d and D_c represent the diffusivity of the species in the secondary and primary liquid phases respectively.

$$D_{eff} = D_c \left[\frac{D_r(1 + 2x_d) + 2(1 - x_d)}{D_r(1 - x_d) + (2 + x_d)} \right]; D_r = \frac{D_d}{D_c} \tag{10}$$

It should be noted that the effective properties defined by Eqs. (9) and (10) can be, in a general sense, regarded as bulk properties. Appropriate as it may be to define them, a full description of mass transfer in a liquid–liquid dispersion also requires an examination of changes introduced by the secondary liquid phase at the mass-transfer interface. Tied to this are the questions whether the secondary liquid phase will be present at the interface and whether it is involved in active uptake of dissolving species at the interface. Indeed, the concept of a pseudo-homogenous liquid implies that the secondary liquid phase will be present, not only in the bulk of the primary liquid, but also at the interface. Furthermore, homogeneity implies that a similar distribution of the secondary liquid phase is found at the interface as is found in the bulk of the primary liquid phase. However, researchers have considered different possible configurations of the interface as illustrated in **Figure 2**. In this way, the requirement for homogeneity has been relaxed at the interface while being maintained in the bulk.

Assuming active uptake by the secondary liquid phase, different possible pathways of mass transfer have arisen. These have included, for example, parallel mass transfer and series mass transfer with or without the shuttling of the droplets of the secondary liquid phase [14, 30, 32, 33]. These various pathways have been associated with an enhancement in mass transfer besides that occurring due to changes discussed earlier

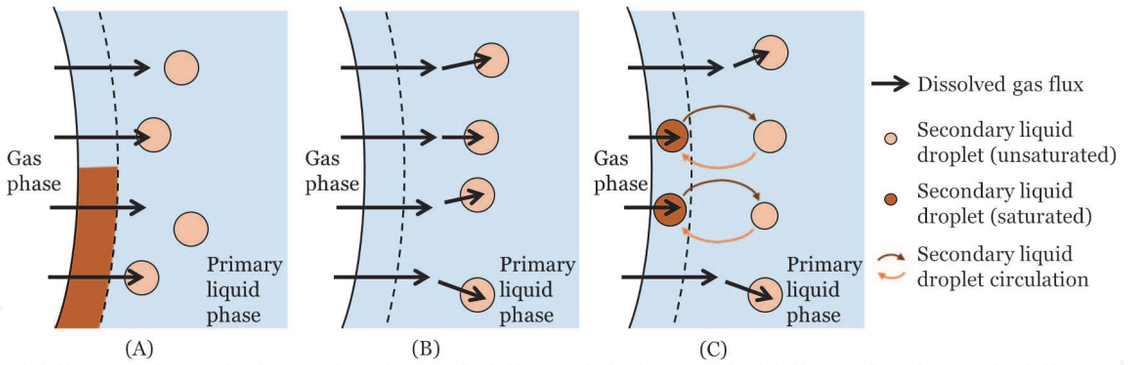

Figure 2.
Mass transfer interface illustrating possible configurations – (A) parallel mass transfer, (B) series mass transfer without shuttling and (C) series mass transfer with shuttling.

(refer to Eq. (9) and (10)). A review of these pathways as well as their associated enhancement factors can be found in the work by Dumont & Delmas [19].

2.3 Changes in reactor hydrodynamics

The hydrodynamics of a reactor are taken to refer to the mean velocity field and the turbulence field within a reactor. These affect mass transfer in various ways. For example, the transport of gas bubbles within a reactor (and hence overall gas hold up) is dependent on the magnitude and orientation of the mean velocity field. Additionally, mass transfer at the interface between the gas bubbles and the liquid phase will depend on the prevailing local turbulence. Consequently, a change in the reactor hydrodynamics will lead to a change in the mass transfer.

The addition of a secondary liquid phase has been observed to change both the mean velocity field and the turbulence levels in stirred tank reactors [34–36]. Direct measurements of the velocity through techniques such as Particle Image Velocimetry [34, 36] and Laser Doppler Anemometry [35] have revealed that a secondary liquid phase can dampen the mean velocities [34, 35] while either increasing or decreasing the turbulence levels [34–36]. Further evidence in literature for a change in the hydrodynamics has been largely indirect – inferred from examining the change in, for example, mixing time upon addition of a secondary liquid phase [37, 38].

Two schools of thought have been postulated to explain the interaction of the secondary liquid phase with the hydrodynamics of a reactor. The first has been focused on the change in effective fluid properties. In this line of thinking, it has been suggested that a decrease in the effective density should lead to an increase in the velocities [34]. On the other hand, it has been suggested that an increase in the effective viscosity should have a dampening effect on both the mean velocities and the turbulence levels [34, 35].

The second school of thought, on the other hand, has been focused on the augmentation or dampening of turbulence by the droplets of the secondary liquid phase [34, 35]. Various mechanisms have been suggested in this regard although these are still the subject of active research [39–42]. For example, whether a particle (solid, liquid or gas) augments or dampens turbulence has been traditionally associated with the size of the particle (d_p) in relation to the integral (or large) scales of turbulence (l) [43]. Large particles ($d_p/l > 0.1$) with characteristically large particle's Reynolds numbers ($Re_p > 400$) have generally been associated with turbulence augmentation through mechanisms such as vortex shedding in the wakes behind the particles [43, 44]. On the other hand, small particles ($d_p/l < 0.1$) have generally

been associated with a dampening of turbulent kinetic energy (TKE) that occurs as the particles are accelerated/dragged by the flow [39, 43].

It should be noted, however, that the above observations do not represent a fixed rule; exceptions have been observed. For example, it has been observed that particles of a size $d_p/l < 0.1$ can both augment and dampen turbulence depending on the flow's Reynolds number [45]. Furthermore, it has been observed that turbulence can be augmented by particles of a size in the order of the Kolmogorov (smallest) scales of turbulence [46–50]. In the latter cases, however, the non-uniform modification of the spectrum of TKE by particles was considered with the augmentation of TKE observed to occur at the small scales of turbulence [46–50]. Mechanisms that were proposed for the turbulence augmentation included flow forcing due to the inertia [50] or buoyancy [49] of small particles that were well correlated with the fluctuating fluid flow.

3. Computational fluid dynamics for gas–liquid–liquid reactors

As illustrated in the previous sections, the introduction of a secondary liquid phase into a traditional gas–liquid reactor can result in a variety of changes. Consequently, the modelling of mass transfer in gas–liquid–liquid reactors requires a comprehensive modelling framework that can account for the different changes. An empirical approach, such as illustrated in Eq. (11) [51], may not suffice as the numerous effects introduced by the secondary liquid phase are reduced into a single term with an adjustable exponent requiring optimisation (compare to Eq. (1)). This is not an easily generalizable approach.

$$K_L a' = \Gamma \cdot \left(\frac{P_g}{V}\right)^x \nu_s^{\,y} (1 - x_d)^z \tag{11}$$

Computational Fluid Dynamics (CFD), on the other hand, offers a fundamental framework that can be built upon to incorporate as much level of detail (or physics) as necessary/desired. This is the case since CFD offers an approximate/numerical solution to the fundamental equations of flow governing a system/reactor [7, 52]. Consequently, the hydrodynamics of a reactor are resolved in space and time and such hydrodynamic data can be coupled to fundamental models of mass transfer so as to predict parameters of interest such as the overall volumetric mass transfer coefficient, $K_L a'$.

As CFD-based approaches are inherently computationally intensive, a major constraint to such approaches is the computational resources available [7, 52]. Thus, a compromise has to be made between the level of physics to be captured and computational resources available [7]. For example, prior consideration must be given as to the level of resolution to be employed for the flow field. Similarly, an appropriate continuum description of the phases involved must be chosen *a priori*. Such compromises notwithstanding, a higher level of detail, accuracy and generality is still maintained with a CFD-based approach in comparison to empirical approaches. This will be illustrated in Section 4.

3.1 Modelling frameworks for hydrodynamics

As noted in the introduction to CFD above, several prior considerations have to be made with regard to the modelling approach. These considerations tend to give rise to different modelling frameworks or techniques. For example, as relates to the

resolution of flow fields, it is possible to simulate the usually turbulent flow in a reactor at all length- and time-scales using Direct Numerical Simulations but the associated computational expense is prohibitive [53]. Therefore, filtering or averaging of the flow field is usually done [53]. Filtering techniques such as those used in Large Eddy Simulations offer an enhanced resolution of the flow field as compared to averaging techniques [53]. However, they are still considered computationally expensive and their use has been largely limited to single-phase reactors [53]. Averaging techniques such as those used to generate the Reynolds-Averaged Navier–Stokes (RANS) equations, on the other hand, lead to tractable simulations [53] and are a practical choice for the modelling of multiphase reactors.

With regard to the description of the phases, an Eulerian framework is typically used for the continuous phase (primary liquid phase) and it involves describing the flow based on a fixed observer position [54]. For the dispersed phases (gas and secondary liquid phase), on the other hand, either an Eulerian framework or a Lagrangian framework can be employed [54]. The Lagrangian framework involves the tracking of individual particles of the dispersed phase within the flow field of the continuous phase [54]. The particles either follow the flow field without interaction (one-way coupling) or interact with it thus modifying it (two-way coupling) [55].

The Lagrangian framework provides a greater degree of detail and as can be expected, it is costly to implement [54]. Consequently, an Eulerian framework for both the continuous and dispersed phases tends to provide a practical choice for modelling. An Eulerian description of both phases assumes that the phases involved can be treated as a continuum [56]. In this case, a phase indicator function is introduced into the governing equations of flow to account for the possible realisation of a phase i at a given position and a given time [56]. Averaging of the governing equations after decomposing the instantaneous flow field into its mean and fluctuating components results in Eq. (12) and (13) [57].

$$\frac{D}{\mathrm{Dt}}(\alpha_i \rho_i) = 0 \tag{12}$$

$$\frac{D}{Dt}\left(\alpha_i \rho_i \overline{V_i}\right) = -\alpha_i \nabla p + \nabla \cdot \bar{\bar{\tau}}_i + \alpha_i \rho_i \bar{g} + \sum_{j=1}^{n} \overline{R}_{ji} \tag{13}$$

In Eqs. (12) and (13), subscripts i and j represent individual phases whereas α represents the respective phase volume fraction. This volume fraction is based on the total volume of all phases as opposed to the total liquid volume (see variable x in earlier equations). The respective phases can be either the gas phase, the primary liquid phase or the secondary liquid phase. Alternatively, if the liquid–liquid dispersion is treated as a pseudo-homogenous liquid, then the subscripts would refer to either the gas phase or the pseudo-homogenous liquid.

Other variables in Eqs. (12) and (13) such as ρ and $\overline{V}$ represent the density and the mean velocity of the respective phases whereas p represents the shared pressure field. Additionally, $\bar{g}$ represents the gravitational acceleration while $\overline{R}$ represents the interphase momentum exchange terms. These terms include the lift force, the drag force, the turbulent dispersion force and the added mass force among others [56].

There are two key points to note regarding the interphase momentum exchange terms. First, their significance varies with the set up being considered. For example, the drag force has been observed to be the most significant interphase exchange term in the bulk of a stirred tank reactor [58, 59]. On the other hand, terms such as the lift force have been observed to significantly affect the flow in a bubble column reactor [60]. Consequently, modelling can be simplified by only accounting for significant terms.

The second point to note touches on the various models that have been proposed to specify the interphase momentum exchange terms. Such models chiefly consider 2-phase interactions, that is, gas–liquid or liquid–liquid interactions [61–63]. Though such models have been improved upon to consider effects such as particle-particle interaction at high volume fractions of a single dispersed phase [61–63], there is still a need for appropriate models that specify the interphase exchange terms when more than two phases are present. To this end, work such as that by Baltussen et al. [64, 65] investigating the effective gas–liquid drag in the presence of an additional solid phase may provide direction.

Finally, $\bar{\bar{\tau}}$ in Eq. (13) represents the stress tensor accounting for both viscous and turbulent (Reynolds') stresses. The specification of the stress tensor is non-trivial due to the Reynolds' stresses that need to be solved directly or modelled. A direct solution of the Reynolds' stresses provides a greater amount of detail and is able to resolve complex features of the turbulence field such as anisotropy [53, 54]. However, the computational costs associated with this approach as well as reported solution difficulties favour the specification of the stress tensor using alternative simplified approaches [53, 54]. Modelling of the stress tensor using the Boussinesq hypothesis is one such alternative approach [53, 54]. In the latter, the Reynolds' stresses are related to the gradients of the mean velocity with the eddy/turbulent viscosity (μ_t) arising as a proportionality constant (see Eq. (14)) [57].

$$\bar{\bar{\tau}}_i = \alpha_i\left(\mu_i + \mu_{t,i}\right)\left(\nabla\overline{V_i} + \nabla\overline{V_i}^T\right) - \frac{2}{3}\alpha_i\left(\left(\mu_i + \mu_{t,i}\right)\nabla\cdot\overline{V_i} + \rho_i k_i\right)\bar{\bar{I}} \tag{14}$$

$$\mu_{t,i} = C_\mu \rho_i \frac{k_i^2}{\epsilon_i} \tag{15}$$

The eddy viscosity can be modelled in various ways such as that illustrated in Eq. (15) [53, 57]. In this case, it is related to the turbulent kinetic energy (k) and its dissipation rate (ϵ), both of which need to be solved for. Various models have been proposed for these latter parameters (k and ϵ) such as the dispersed k–ϵ turbulence model, the mixture k–ϵ turbulence model and the per-phase k–ϵ turbulence model [57]. These models represent an extension of the single phase k–ϵ turbulence model to multiphase situations and their applicability depends on the expected/prevailing type of flow [57]. For example, the mixture k–ϵ model is recommended for stratified flow whereas the dispersed k–ϵ model is recommended where there is one clear continuous phase and the other phases are dispersed within it [57].

It should be noted that irrespective of the choice of turbulence model, one key point to consider is the interaction of the dispersed phases with the prevailing turbulence. As noted in Section 2.3, the dispersed phase can modify the prevailing turbulence and this needs to be captured. To this end, various models have been proposed in literature and these vary in complexity depending on the level of detail captured. Various authors have recently examined the sufficiency of these models and their work is recommended [66–71].

3.2 Modelling frameworks for mass transfer

Similar to the modelling of hydrodynamics, the modelling of mass transfer involves the selection of appropriate frameworks prior to the actual simulation. The choice of a particular framework involves a compromise between the level of detail captured and computational cost involved. Furthermore, the choice of a modelling framework for mass transfer tends to be influenced by choices made during the

modelling of the hydrodynamics. For example, the use of an Eulerian description of the phases together with averaged equations of flow offers a practical choice for the modelling of a reactor hydrodynamics. However, this approach involves a loss of specifics on the mass transfer interface thus necessitating the prescription of models to approximate the expected mass transfer behaviour. On the other hand, a Lagrangian tracking of particles coupled with interface tracking algorithms better resolves the mass transfer interface but is unfeasible for reactors with a large number of dispersed particles (droplets or bubbles). Consequently, the discussion below focuses on the modelling of mass transfer within the context of an Eulerian description of the phases and the modelling of hydrodynamics using averaged equations of flow.

Mass transfer in a gas–liquid–liquid reactor can be solved for by tracking the concentration of a species in each phase within the reactor. This results in three equations as given in Eqs. (16)–(18). In these equations, C represents the concentration of the species in the respective phase (subscripts g, c, d) whereas $\bar{J}$ and S represent the diffusive flux and the interphase mass transfer source terms respectively. Closure models are required for the interphase mass transfer source terms depending on the expected mass transfer behaviour.

$$\frac{D}{Dt}\left(\alpha_g C_g\right) = -\nabla \cdot \left(\alpha_g \bar{J}_g\right) - \mathrm{S}_{gc} - \mathrm{S}_{gd} \tag{16}$$

$$\frac{D}{Dt}\left(\alpha_c C_c\right) = -\nabla \cdot \left(\alpha_c \bar{J}_c\right) + \mathrm{S}_{gc} - \mathrm{S}_{cd} \tag{17}$$

$$\frac{D}{Dt}\left(\alpha_d C_d\right) = -\nabla \cdot \left(\alpha_d \bar{J}_d\right) + \mathrm{S}_{gd} + \mathrm{S}_{cd} \tag{18}$$

In the most general case, mass transfer can be assumed to occur between the gas phase and both the primary and the secondary liquid phases ($\mathrm{S}_{gc} \neq 0, \mathrm{S}_{gd} \neq 0$). This would correspond to the case of parallel mass transfer as illustrated in **Figure 2(A)**. Evidence for this mass transfer pathway has been provided based on observations of the formation by oil films on gas bubbles during "static" experiments [72]. The question arises, however, as to whether sufficient time for film formation occurs in a dynamic/agitated reactor [72, 73].

Series mass transfer is often taken to be the more probable mass transfer pathway in an agitated reactor (cases (B) or (C) in **Figure 2** with $\mathrm{S}_{gd} = 0$) [34]. In addition, the formation of small droplets of the secondary liquid phase with a large interfacial area implies that mass transfer between the respective liquid phases is usually faster than that occurring between the gas phase and the primary liquid phase [72]. Thus, based on the timescale of mass transfer between the gas phase and the primary liquid phase, it may be assumed that equilibrium conditions exist between the respective liquid phases. Furthermore, one need only track the concentration of the species in two phases – the gas phase (Eq. (16)) and the primary liquid phase (Eq. (17) with $\mathrm{S}_{cd} = 0$). With these simplifying assumptions, the only unknown left is the interphase source term between the gas phase and the primary liquid phase (S_{gc}). Gakingo et al. [13, 28] proposed definitions for S_{gc} that account for possible mass transfer pathways at the gas–liquid interface plus an apparent decrease in the overall volumetric mass transfer coefficients that occurs due to a larger total solubility of the species in the liquid–liquid dispersion (refer to Section 2.2). This illustrated in Eqs. (19)–(21) below [13, 28].

$$\mathrm{S}_{gc} = K_L a' \left(C_c^* - C_c\right) \tag{19}$$

$$K_L a' \approx E' \cdot \Lambda \cdot \sqrt{D_c}\left(\frac{\rho_c \epsilon_c}{\mu_c}\right)^{0.25} \cdot \left(\frac{6\alpha_g}{d_g}\right) \tag{20}$$

$$E' = \frac{1}{(1 - \alpha_d + \alpha_d m)^{\varphi}} \tag{21}$$

In the equations above, $K_L a'$ represents the overall volumetric mass transfer coefficient in the presence of the secondary liquid phase. The latter has been expanded in Eq. (20) based on an eddy cell model [74] with Λ and E' representing a constant and the enhancement factor respectively. The enhancement factor is given in Eq. (21) where m represents the solubility ratio ($m = C_d^* / C_c^*$) and the exponent φ varies between 0.5 and 1. A value of $\varphi = 1$ represents the series mass transfer pathway without shuttling whereas a value of $\varphi = 0.5$ represents the series mass transfer pathway with shuttling [13, 28]. Other variables are as previously defined.

4. Case studies

Few studies have reported on the CFD-based modelling of gas–liquid–liquid reactors. Two such studies are reviewed in this section with the one having focussed on the modelling of mixing time [12] while the other focussed on the modelling of mass transfer [13].

In the case studies of interest, stirred tank reactors were considered as illustrated in **Table 3**. In addition, the modelling in both cases was done based on an Eulerian description of the phases involved (refer to Eqs. (12) and (13)). There were certain similarities in the modelling and these included, for example, a consideration of drag force as the only interphase momentum exchange term. The latter was specified according to Eq. (22) [13] with different models for the drag coefficient (C_D) employed as illustrated in **Table 4**. Constant sizes were also assumed for both the gas phase bubbles and the droplets of the secondary liquid phase and these were predicted by Eqs. (3) and (23) respectively [12, 13]. Finally, turbulence was modelled based on the dispersed k–ϵ model (see Eqs. (24) and (25)) though the use of the Reynolds stress model was additionally considered in one study [12].

Experimental details		**Cheng et al. [12]**	**Gakingo et al. [13]**
Tank dimensions	Tank diameter	0.24 m	0.177 m
	Liquid height	0.24 m	0.22 m
	Impeller diameter	0.08 m	0.059 m
	Number of impellers	1	2
Aeration system	Sparger diameter	0.08 m	0.05 m
	Sparger holes (diameter)	16 (0.0015 m)	7 (0.001 m)
Operating conditions	Agitation rates (rpm)	170, 220, 300, 400, 425, 500	600, 800
	Aeration rates (L/min)	0.16, 0.24, 0.32, 0.4, 0.48, 0.64	4
	Primary liquid phase	Water	Water
	Secondary liquid phase (volume fractions)	Kerosene (0%, 3%, 5%, 7%, 10%, 12%, 15%, 20%)	n-C_{10}-C_{13} alkane cut (0%, 2.5%, 5%, 10%, 20%)

Table 3.
Details of experimental setups used in the studies of Cheng et al. [12] and Gakingo et al. [13].

Parameter	Cheng et al. [12]	Gakingo et al. [13]
Gas phase–primary liquid phase drag coefficient (with correction for turbulence effects)	$C_{D,\infty} = max\left\{\begin{array}{l}\frac{2.667Eo}{Eo+4},\\ \frac{24}{Re_p}\left(1+0.15Re_p^{0.687}\right)\end{array}\right\}$	$C_{D,\infty}^{sph} = \frac{24}{Re_p}\left(1+0.1Re_p^{0.75}\right);$ $C_{D,\infty}^{ell} = \frac{2}{3}d_g\left(\frac{g\Delta\rho}{\sigma_{gc}}\right)^{0.5}\left(\frac{1+17.67\left(1-\alpha_g\right)^{1.29}}{18.67\left(1-\alpha_g\right)^{1.5}}\right)^2;$ $C_{D,\infty}^{cap} = \frac{8}{3}\left(1-\alpha_g\right)^2;$
	$\frac{C_D}{C_{D,\infty}} - 1 = 6.5\times10^{-6}\left(\frac{d_g}{\lambda}\right)^3$	$\frac{C_D}{C_{D,\infty}} = \Theta\times\left[1-1.4St^{0.7}\exp\left(-0.6\,St\right)\right]^{-2}$
Secondary liquid phase–primary liquid phase drag coefficient	$C_D = C_{D,\infty} = \left(1+\alpha_d^{1/3}\right)\left(0.63+\frac{4.8}{\sqrt{Re_p}}\right)^2$	$C_D = C_{D,\infty} = \left\{\begin{array}{ll}\frac{24}{Re_p}\left(1+0.15Re_p^{0.687}\right); & Re_p \le 1000\\ 0.44; & Re_p > 1000\end{array}\right.$
Turbulence modulation by dispersed phases	$\Pi_{k_c} = 0.02\times\left\|\overline{R}_{ci}\right\|\sqrt{\left(\overline{\mathrm{V}}_i-\overline{\mathrm{V}}_c\right)^2}$	$\Pi_{k_c} = \frac{\rho_i}{\rho_i+C_{AM}\rho_c}\times\frac{K_{ic}}{\alpha_c\rho_c}\left[\zeta_{ic}-2k_c+\overline{\mathrm{V}}_{dr}\bullet\left(\overline{\mathrm{V}}_i-\overline{\mathrm{V}}_c\right)\right]$
	$\Pi_{\epsilon_c} = C_{1\epsilon}\frac{\epsilon_c}{k_c}\Pi_{k_c}$	$\Pi_{\epsilon_c} = C_{3\epsilon}\frac{\epsilon_c}{k_c}\Pi_{k_c}$

Table 4.
Sub-models used in the modelling work of Cheng et al. [12] and Gakingo et al. [13].

$$\overline{R}_{ji} = -\overline{R}_{ij} = K_{ji}\left(\overline{\mathrm{V}}_j-\overline{\mathrm{V}}_i\right); K_{ji} = \frac{3}{4}\alpha_i\alpha_j\rho_i\frac{C_D}{d_j}\left|\overline{\mathrm{V}}_j-\overline{\mathrm{V}}_i\right| \tag{22}$$

$$\frac{d_d}{T} = \Omega\cdot\left(1+\gamma\cdot\alpha_{o,ave}\right)\left(\frac{\sigma_{cd}}{\rho_c N^2T^3}\right)^{0.6} \tag{23}$$

$$\frac{D}{Dt}\left(\alpha_c\rho_c k_c\right) = \nabla\cdot\left(\alpha_c\left(\mu_c+\frac{\mu_{t,c}}{\sigma_k}\right)\nabla k_c\right)+\alpha_c G_{k,c}-\alpha_c\rho_c\epsilon_c+\alpha_c\rho_c\Pi_{k_c} \tag{24}$$

$$\frac{D}{Dt}\left(\alpha_c\rho_c\epsilon_c\right) = \nabla\cdot\left(\alpha_c\left(\mu_c+\frac{\mu_{t,c}}{\sigma_\epsilon}\right)\nabla\epsilon_c\right)+\alpha_c\frac{\epsilon_c}{k_c}\left(C_{1\epsilon}G_{k,c}-C_{2\epsilon}\rho_c\epsilon_c\right)+\alpha_C\rho_c\Pi_{\epsilon_c} \tag{25}$$

The above similarities, notwithstanding, there were some notable differences between the two studies. For example, Gakingo et al. [13] tested two approaches in the modelling of the liquid–liquid dispersion. The first approach involved the treatment of the dispersion as a pseudo-homogenous liquid (herein referred to as the P-HOM approach) and the mixture properties were obtained from Eq. (5) for effective density or through experimental measurements for effective viscosity. The second approach, also used by Cheng et al. [12], involved a consideration of the heterogeneous nature of the dispersion and a modelling of each individual liquid phase (herein referred to as the HET approach). In this second approach, there was a need to specify models for turbulence modulation by the dispersed phases (Π_{k_c} in Eq. (24)) and different models were employed as illustrated in **Table 4**. Last but not least, mass transfer was considered in only one study [13] where the authors employed the previously reviewed frameworks, that is, Eqs. (16) and (17) with $S_{gd} = 0$, $S_{cd} = 0$ and Eqs. (19)–(21). Further specifics on the implementation of the modelling approaches (meshing, boundary conditions and solver settings) can be found in the respective studies [12, 13].

Several key observations can be made from the reported modelling works [12, 13]. First, it was observed that the hydrodynamics of a gas–liquid–liquid stirred tank reactor were better captured based on the HET modelling approach as opposed to the P-HOM modelling approach [13]. The failure by the latter approach was attributed to the fact that the hydrodynamics in a turbulent stirred tank reactor are

dominated by turbulence as opposed to the effective (mixture) viscosity. To this end, it was reported that the ratio of turbulence viscosity to mixture viscosity was in the order of $O(10-100)$ based on the P-HOM modelling approach [13]. Consequently, a minimal change in the hydrodynamics was observed despite an almost 2-fold increase in the values of mixture viscosity [13]. This is illustrated through the minimal change in gas hold up trends shown in **Figure 3**.

As pertains to the HET modelling approach, the better performance at capturing the hydrodynamics and hence gas hold up trends (see **Figure 3**) was attributed to the capture of turbulence modulation by droplets of the secondary liquid phase [13]. In particular, it was reported that there was an increase in the turbulence viscosity which served to dampen the mean velocity field (see **Figure 4**) thus reducing the effective drag and dispersion experienced by the gas bubbles [13]. Cheng et al. [12], on the other hand, did not make an explicit mention of changes in the turbulence viscosity. Rather, they hypothesised that their mixing time was reduced at low volume fractions of the secondary liquid phase due to an increase in turbulence caused by the droplets of the latter [12]. Furthermore, they hypothesised that an increase in mixing time at high volume fractions of the secondary liquid phase was due to a dampening of the turbulence arising from an increase in the effective viscosity [12]. This reference to notable changes due to the effective viscosity stands in contrast with the findings on the P-HOM modelling approach [13].

A recent study on a gas–liquid–solid reactor has reported similar gas hold up trends as those reported for the HET approach [75]. Furthermore, the modelling of such a reactor based on non-Newtonian models for the liquid–solid slurry has been observed to result in the formation of regions of localised fluid motion near the impeller (caverns) with stagnant fluid elsewhere in the tank [75, 76]. This corresponds to the reports of a dampened mean velocity field according to the HET approach as seen in **Figure 4**. Observations such as these suggest that the dampening of the mean velocity field may be a common feature in three-phase reactors. However, questions arise as to the appropriate manner of describing such effects. For example, the question may be posed as to whether liquid–liquid dispersions in stirred tanks should be treated based on non-Newtonian models with a yield stress and shear-thinning behaviour rather than equations of the type given in Section 2.1 (Eqs. (6)–(8)). It is to be noted that Eqs. (6)–(8) predict the effective viscosity of the dispersion assuming no non-Newtonian behaviour. Furthermore, the

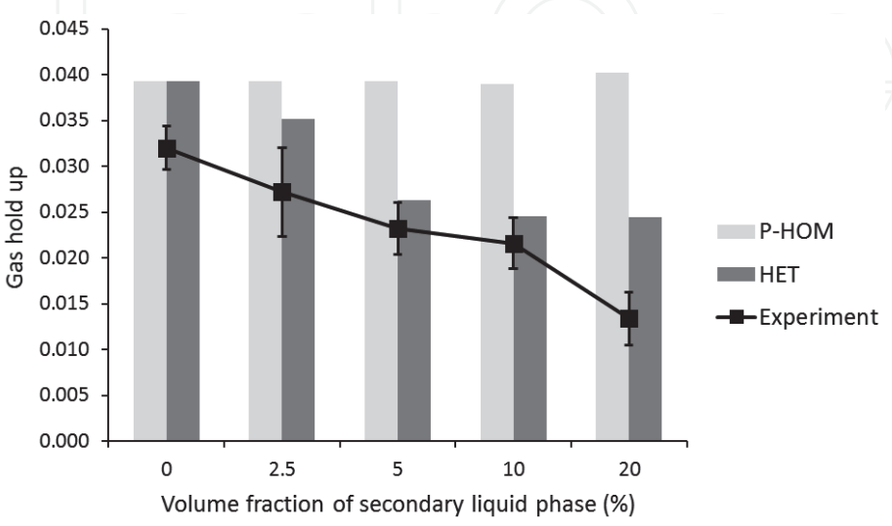

Figure 3.
Gas hold up versus volume fraction of secondary liquid phase at 600 rpm. P-HOM refers to the pseudo-homogenous modelling approach whereas HET refers to the individual treatment of the liquid phases. Data from Gakingo et al. [13].

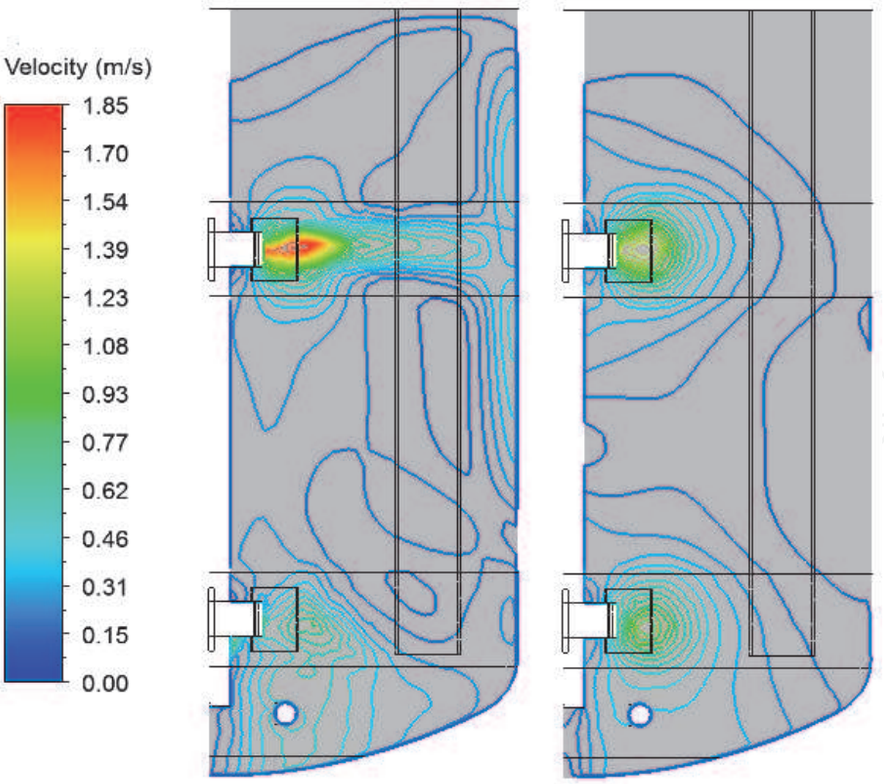

Figure 4.
Velocity contours based on the HET modelling approach on a mid-baffle plane at 600 rpm. Left – 0% alkane volume fraction (2-phase). Right –10% alkane volume fraction.

experimental effective viscosity values that were used for the P-HOM modelling approach were in close agreement with those predicted by these equations [13].

Further observations made in the case studies of interest touched on the trends of pumping capacity and power drawn by the impellers. It was observed that the pumping capacity of the impellers decreased at high volume fractions of the secondary liquid phase [12, 13]. This was attributed to a decrease in the mean velocity field as dissipated by an increasing turbulence viscosity [13]. As for the power drawn, both an increase and a decrease in the power was reported. The decrease in power, as noted by Cheng et al. [12], was attributed to a decrease in the effective density upon addition of the secondary liquid phase. On the other hand, Gakingo et al. [13] attributed a noted increase in power drawn to increased energy dissipation by the droplets of the secondary liquid phase. This latter effect was not reported by Cheng et al. [12] and this could have been due to the use of different models to capture turbulence modulation by the dispersed phases (see **Table 4**). Cheng et al. [12] used a model by Katoaoka et al. [77] which considers only the mean velocity differences $\left(\overline{V_i} - \overline{V_c}\right)$ in computing the work done by interfacial drag. Gakingo et al. [13], on the other hand, employed the model by Simonin et al. [57, 78–80] which considers not only the effects arising from mean velocity differences but also the effects arising from the fluctuating velocities of the dispersed phase particles. These latter effects were expected to become more significant than the former as the size of the dispersed phase particles decreased $(\overline{V_i} - \overline{V_c} \to 0 \text{ as } d_p \to 0)$ [68]. Consequently, it may be suggested that the use of the model by Simonin et al. [57, 78–80] was more appropriate as it is more comprehensive.

With regard to mass transfer, it was illustrated that potentially accurate predictions can be obtained by using the HET modelling approach for hydrodynamics

and Eqs. (16), (17) and (19)–(21) for mass transfer with $S_{gd} = S_{cd} = 0$ (see **Figure 5**) [13]. These equations correspond to a case where the concentrations of a species in the two liquid phases are at equilibrium and no direct uptake by the secondary liquid phase occurs at the gas–liquid interface. Though this scenario implied the occurrence of either series mass transfer or series mass transfer with shuttling, minimal differences were reported based on a consideration of these two

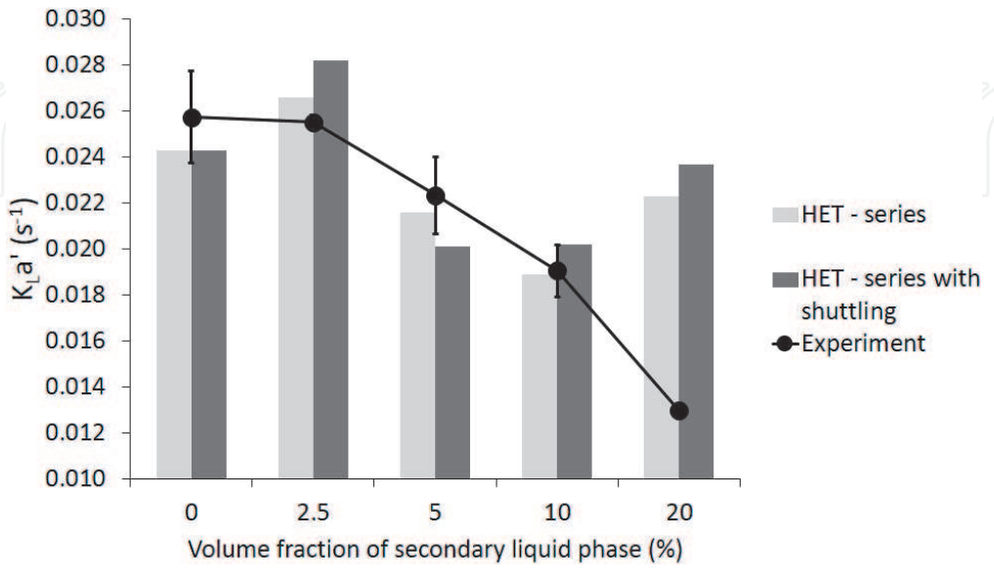

Figure 5.
Comparison of predicted versus experimental overall volumetric mass transfer coefficients at 600 rpm and varying alkane concentrations. Experimental measurements have been obtained by the pressure step method. Data from Gakingo et al. [13].

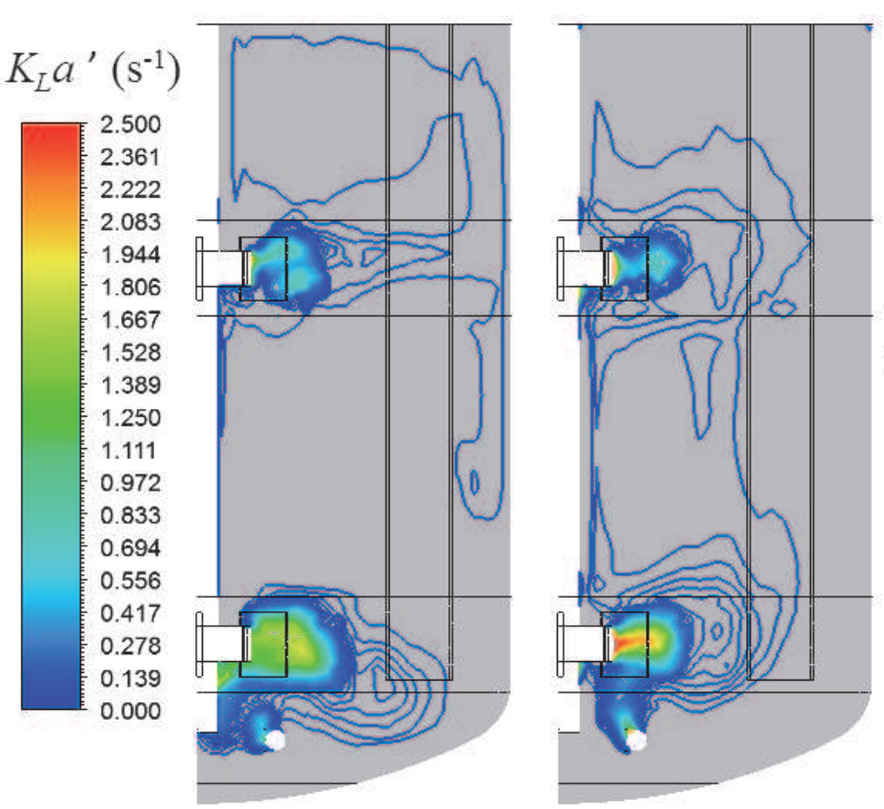

Figure 6.
Contours of local K_La' values predicted based on the HET modelling approach on a mid-baffle plane at 600 rpm. Left – 0% alkane volume fraction (2-phase). Right –10% alkane volume fraction.

alternatives [13]. Thus, it may be suggested that mass transfer in gas–liquid–liquid reactors is less sensitive to the assumed configuration at the gas–liquid interface and more sensitive to other varying parameters such as the energy dissipation rate and the gas hold up. More evidence for or against this suggestion should, however, be provided based on a re-examination of mass transfer using a different set of modelling assumptions.

In conclusion, the usefulness of a CFD-based mass transfer model may be glimpsed from the amount of detail that it can generate. For example, spatial resolutions of variables of interest can be quickly generated as illustrated in **Figure 6** to support the visualisation of changes made during *in situ* reactor design. This is indeed the chief advantage of a CFD-based approach over an empirical approach. However, before the full potential of the CFD-based approach can be realised, a number of areas will need improvement or further investigation. More on this is presented in the subsequent section.

5. Areas requiring further investigation

The results reviewed in the previous section illustrate that the addition of a secondary liquid phase can have a great impact on both the hydrodynamics and the mass transfer in a reactor. In particular, the results suggest that turbulence modulation by the secondary liquid phase is the key mechanism of action through which changes in a reactor occur. A CFD-based framework that is able to capture this mechanism of action has also been proposed and its potential has been illustrated. This notwithstanding, care ought to be taken in generalising the results obtained and the implications arising from them. This is because there still are a number of issues that need further investigation. Two such pertinent issues are highlighted below.

The first pertinent issue concerns the applicability of the obtained results to different reactors. It is the view of the authors that the results reported above should be taken as being particular to stirred tank reactors operating in the turbulent regime. This would be in line with existing experimental evidence for turbulence modulation by secondary liquid phases in turbulent stirred tank reactors [34–37]. Different reactors, on the other hand, may have alternative mechanisms of action. For example, recent studies in a gas–liquid–liquid–solid bubble column reactor have illustrated that the addition of a secondary liquid phase did not significantly impact the hydrodynamics of the reactor [81, 82]. Rather, a greater impact on the hydrodynamics was observed for the solid phase and this depended on the type of the solid phase employed [81, 82]. Consequently, it may be suggested that a pseudo-homogenous treatment of the liquid–liquid dispersion would suffice for such a bubble column reactor contrary to what has been established in the case study above.

The second point worth investigation is the sensitivity of CFD-based results to the sub-models and simplifying assumptions employed. As noted in sections 3.1 and 3.2, quite a number of decisions have to be made prior to the actual simulations. Though these decisions are necessitated by a need to keep the simulations tractable, the quality of results obtained may be impacted. It is the view of the authors that particular attention should be given to the sub-models used to capture turbulence modulation. This is because of the seemingly large effects that turbulence modulation had on the results presented in the case study. To this end, it is recommended that comprehensive sets of experiments should be conducted on gas–liquid–liquid reactors and these should involve a concurrent measurement of the mass transfer and the hydrodynamics. Current literature is fragmented with authors who have

investigated mass transfer not having measured the potential changes in the hydrodynamics and vice versa.

Acknowledgements

The authors would like to acknowledge Ayman A. Abufalgha for performing the surface tension measurements.

The first author would also like to acknowledge funding received from the DST-NRF Centre of Excellence in Catalysis (c*change) and the DAAD-AIMS In Region Scholarship Programme.

Nomenclature

d	Diameter (m).
$\bar{g}$,g	Gravitational acceleration vector, gravitational constant (m/s^2).
k	Turbulent kinetic energy (m^2/s^2).
l	Integral length scale of turbulence.
m	ratio of concentration of a species dissolved in secondary liquid phase to that dissolved in primary liquid phase at equilibrium.
n	Total number of phases.
ν_s	Superficial gas velocity (m/s).
x_g	Volume fraction of gas phase based on total volume in a gas–liquid reactor.
x_d	Volume fraction of secondary liquid phase based on total volume of un-gassed reactor.
x_m	Maximum packing limit.
C	Dissolved concentration of a species (mol/m^3).
C^*	Dissolved saturation concentration of a species (mol/m^3).
C_D	Drag coefficient.
$C_{D,\infty}$	Drag coefficient in the absence of turbulence.
D	Diffusivity of a species in a liquid phase (m^2/s).
D_r	Diffusivity ratio
E'	Enhancement factor.
Eo	Eotvos number.
$\bar{\bar{I}}$	Identity tensor.
$\bar{J}$	Total diffusive flux of a species.
$G_{k,c}$	Production of turbulent kinetic energy from mean velocity gradients.
K_La	Overall volumetric mass transfer coefficient in the absence of a secondary liquid phase (s^{-1}).
K_La'	Overall volumetric mass transfer coefficient in the presence of a secondary liquid phase (s^{-1}).
K_{ji}	Interphase momentum exchange coefficient between phases i and j.
N	Impeller speed (rps).
P_g	Gassed power (W).
Re	Reynolds number.
St	Stokes number.
T	Impeller diameter (m).

V	Volume (m^3).
$\overline{V}$	Velocity vector (m/s).
$\overline{V}_{dr}$	Drift velocity (m/s).
α	Volume fraction based on total volume in a gassed reactor.
ϵ	Turbulent kinetic energy dissipation rate (m^2/s^3).
ρ	Density (kg/m^3).
σ	Surface/interfacial tension (N/m).
$\bar{\bar{\tau}}$	Stress tensor (Pa).
μ	Dynamic viscosity (Pa s).
μ_t	Turbulent viscosity (Pa s).
μ_r	Viscosity ratio.
λ	Kolmogorov length scale.
ζ_{ic}	Covariance of fluctuating velocities between phase i and the continuous liquid phase (subscript c).
Π_{k_c}	Production (destruction) of turbulent kinetic energy by motion of dispersed particles.
Π_{ϵ_c}	Production (destruction) of turbulent kinetic energy dissipation rate by motion of dispersed particles.
x, y, z, φ	Exponents.
$\Gamma, \Lambda, \gamma, \Omega, \Theta, C_\mu$ $\sigma_k, \sigma_\epsilon, C_{1\epsilon}, C_{2\epsilon}$ $C_{3\epsilon}, C_{AM}$	Constants.

Subscripts/superscripts

c	Continuous/primary liquid phase.
d	Secondary liquid phase.
g	Gas phase.
p	Dispersed particle (gas, liquid or solid).
i, j	Phases i, j.
cap	Spherical cap.
ell	Elliptical shape.
eff	Effective.
sph	Spherical shape.
sat	Saturated.

Author details

Godfrey Kabungo Gakingo and Tobias Muller Louw*
Department of Process Engineering, Stellenbosch University, Stellenbosch, South Africa

*Address all correspondence to: tmlouw@sun.ac.za

References

[1] Kasat GR, Pandit AB. Review on mixing characteristics in solid-liquid and solid-liquid-gas reactor vessels. Canadian Journal of Chemical Engineering. 2005;83:618–43. DOI: 10.1002/cjce.5450830403.

[2] Karimi M. CFD analysis of solid-liquid-gas interactions in flotation vessels [PhD thesis]. Stellenbosch University, 2014.

[3] Muñoz R, Daugulis AJ, Hernández M, Quijano G. Recent advances in two-phase partitioning bioreactors for the treatment of volatile organic compounds. Biotechnology Advances. 2012;30:1707–20. DOI: 10.1016/j.biotechadv.2012.08.009.

[4] Clarke KG, Correia LDC. Oxygen transfer in hydrocarbon-aqueous dispersions and its applicability to alkane bioprocesses: A review. Biochemical Engineering Journal. 2008; 39:405–29. DOI:10.1016/j. bej.2007.11.020.

[5] Garcia-Ochoa F, Gomez E. Bioreactor scale-up and oxygen transfer rate in microbial processes: An overview. Biotechnology Advances. 2009;27:153–76. DOI:10.1016/j.biotechadv.2008. 10.006.

[6] Besagni G, Inzoli F, Ziegenhein T. Two-Phase Bubble Columns: A Comprehensive Review. ChemEngineering. 2018;2:13. DOI: 10.3390/chemengineering2020013.

[7] Joshi JB, Nandakumar K. Computational modelling of multiphase reactors. Annual Review of Chemical and Biomolecular Engineering. 2015;6: 347–78. DOI:10.1146/annurev-chembioeng-061114-123229.

[8] Sajjadi B, Raman AAA, Ibrahim S, Shah RSSRE. Review on gas-liquid mixing analysis in multiscale stirred vessel using CFD. Reviews in Chemical Engineering. 2012;28:171–89. DOI: 10.1515/revce-2012-0003.

[9] Sajjadi B, Raman AAA, Shah RSSRE, Ibrahim S. Review on applicable breakup/coalescence models in turbulent liquid-liquid flows. Reviews in Chemical Engineering. 2013;29:131–58. DOI:10.1515/revce-2012-0014.

[10] Shah RSSRE, Sajjadi B, Raman AAA, Ibrahim S. Solid-liquid mixing analysis in stirred vessels. Reviews in Chemical Engineering. 2015;31:119–47. DOI: 10.1515/revce-2014-0028.

[11] Wang G, Ge L, Mitra S, Evans GM, Joshi JB, Chen S. A review of CFD modelling studies on the flotation process. Minerals Engineering. 2018;127: 153–77. DOI:10.1016/j.mineng.2018. 08.019.

[12] Cheng D, Wang S, Yang C, Mao ZS. Numerical Simulation of Turbulent Flow and Mixing in Gas-Liquid-Liquid Stirred Tanks. Industrial and Engineering Chemistry Research. 2017; 56:13050–63. DOI:10.1021/acs. iecr.7b01327.

[13] Gakingo GK, Clarke KG, Louw TM. A numerical investigation of the hydrodynamics and mass transfer in a three-phase gas-liquid-liquid stirred tank reactor. Biochemical Engineering Journal. 2020;157. DOI:10.1016/j. bej.2020.107522.

[14] Linek V, Beneš P. A study of the mechanism of gas absorption into oil-water emulsions. Chemical Engineering Science. 1976;31:1037–46. DOI:10.1016/ 0009-2509(76)87024-8.

[15] Clarke KG, Williams PC, Smit MS, Harrison STL. Enhancement and repression of the volumetric oxygen transfer coefficient through hydrocarbon addition and its influence

on oxygen transfer rate in stirred tank bioreactors. Biochemical Engineering Journal. 2006;28:237–42. DOI:10.1016/j.bej.2005.11.007.

[16] Ngo TH, Schumpe A. Oxygen absorption into stirred emulsions of n-alkanes. International Journal of Chemical Engineering. 2012;2012:1–7. DOI:10.1155/2012/265603.

[17] Dumont E, Andrès Y, Le Cloirec P. Mass transfer coefficients of styrene and oxygen into silicone oil emulsions in a bubble reactor. Chemical Engineering Science. 2006;61:5612–9. DOI:10.1016/j.ces.2006.04.026.

[18] Kundu A, Dumont E, Duquenne A-M, Delmas H. Mass transfer characteristics in gas-liquid-liquid system. Canadian Journal of Chemical Engineering. 2003;81:640–6. DOI: 10.1002/cjce.5450810341.

[19] Dumont E, Delmas H. Mass transfer enhancement of gas absorption in oil-in-water systems: A review. Chemical Engineering and Processing: Process Intensification. 2003;42:419–38. DOI: 10.1016/S0255-2701(02)00067-3.

[20] Dumont É. Mass transport phenomena in multiphasic gas/water/NAP systems. Advances in Chemical Engineering. 2019;54:1–51. DOI: 10.1016/bs.ache.2018.12.001.

[21] Correia LDC, Aldrich C, Clarke KG. Interfacial gas-liquid transfer area in alkane-aqueous dispersions and its impact on the overall volumetric oxygen transfer coefficient. Biochemical Engineering Journal. March 2010;49: 133–7. DOI:10.1016/j.bej.2009.12.007.

[22] Littel RJ, Versteeg GF, Van Swaaij WPM. Physical absorption of CO2 and propene into toluene/water emulsions. AIChe Journal. 1994;40: 1629–38.

[23] Pal R. Rheology of simple and multiple emulsions. Current Opinion in Colloid and Interface Science. 2011;16: 41–60. DOI:10.1016/j.cocis.2010.10.001.

[24] Pal R. Novel viscosity equations for emulsions of two immiscible liquids. Journal of Rheology. 2001;45:509–20. DOI:10.1122/1.1339249.

[25] Pal R. Viscous behavior of concentrated emulsions of two immiscible Newtonian fluids with interfacial tension. Journal of Colloid and Interface Science. 2003;263:296–305. DOI:10.1016/S0021-9797(03)00125-5.

[26] Ho CS, Ju L-K, Baddour RF. Enhancing penicillin fermentations by increased oxygen solubility through the addition of n-hexadecane. Biotechnology and Bioengineering. 1990;36:1110–8. DOI:10.1002/bit.260361106.

[27] Littlejohns J V., Daugulis AJ. Oxygen transfer in a gas-liquid system containing solids of varying oxygen affinity. Chemical Engineering Journal. 2007;129:67–74. DOI:10.1016/j.cej.2006.11.002.

[28] Gakingo GK, Louw TM, Clarke KG. Modelling of the overall volumetric mass transfer coefficient measured by the dynamic method in gas-liquid-liquid systems. In: 13th International Conference on Heat Transfer, Fluid Mechanics and Thermodynamics; 2017; Portoroz, Slovenia: p. 662–6.

[29] Dumont E, Andrès Y, Cloirec P Le. Mass transfer coefficients of styrene into water/silicone oil mixtures: New interpretation using the “equivalent absorption capacity” concept. Chemical Engineering Journal. 2014; 237:236–41. DOI:10.1016/j.cej.2013.10.021.

[30] Chawla H, Khanna R, Nigam KDP, Adesina AA. A homogeneous model for mass transfer enhancement in gas-liquid-liquid systems. Chemical Engineering Communications. 2008;

195:622–43. DOI:10.1080/00986440701555431.

[31] Wenmakers PWAM, Hoorn JAA, Kuipers JAM, Deen NG. Gas-liquid mass transfer enhancement by catalyst particles, a modelling study. Chemical Engineering Science. 2016;145:233–44. DOI:10.1016/j.ces.2016.01.043.

[32] Bruining WJ, Joosten GEH, Beenackers AACM, Hofman H. Enhancement of gas-liquid mass transfer by a dispersed second liquid phase. Chemical Engineering Science. 1986;41:1873–7. DOI:10.1016/0009-2509(86)87066-X.

[33] Van Ede CJ, Van Houten R, Beenackers AACM. Enhancement of gas to water mass transfer rates by a dispersed organic phase. Chemical Engineering Science. 1995;50:2911–22. DOI:10.1016/0009-2509(95)00133-P.

[34] Svensson FJE, Rasmuson A. PIV measurements in a liquid-liquid system at volume percentages up to 10% dispersed phase. Experiments in Fluids. 2006;41:917–31. DOI:10.1007/s00348-006-0211-0.

[35] Svensson FJE, Rasmuson A. LDA-measurements in a stirred tank with a liquid-liquid system at high volume percentage dispersed phase. Chemical Engineering and Technology. 2004;27:335–9. DOI:10.1002/ceat.200401981.

[36] Laurenzi F, Coroneo M, Montante G, Paglianti A, Magelli F. Experimental and computational analysis of immiscible liquid-liquid dispersions in stirred vessels. Chemical Engineering Research and Design. 2009;87:507–14. DOI:10.1016/j.cherd.2008.12.007.

[37] Zhao Y, Li X, Cheng J, Yang C, Mao ZS. Experimental study on liquid-liquid macromixing in a stirred tank. Industrial and Engineering Chemistry Research. 2011;50:5952–8. DOI:10.1021/ie102270p.

[38] Cheng D, Cheng J, Li X, Wang X, Yang C, Mao Z. Experimental study on gas-liquid-liquid macro-mixing in a stirred tank. Chemical Engineering Science. 2012;75:256–66. DOI:10.1016/j.ces.2012.03.035.

[39] Balachandar S, Eaton JK. Turbulent Dispersed Multiphase Flow. Annual Review of Fluid Mechanics. 2010;42:111–33. DOI:10.1146/annurev.fluid.010908.165243.

[40] Mathai V, Lohse D, Sun C. Bubbly and Buoyant Particle-Laden Turbulent Flows. Annual Review of Condensed Matter Physics. 2020;11:529–59. DOI:10.1146/annurev-conmatphys-031119-050637.

[41] Poelma C, Ooms G. Particle-Turbulence Interaction in a Homogeneous, Isotropic Turbulent Suspension. Applied Mechanics Reviews. 2006;59:78–89. DOI:10.1115/1.2130361.

[42] Gai G, Hadjadj A, Kudriakov S, Thomine O. Particles-induced turbulence: A critical review of physical concepts, numerical modelings and experimental investigations. Theoretical and Applied Mechanics Letters. 2020;10:241–8. DOI:10.1016/j.taml.2020.01.026.

[43] Gore RA, Crowe CT. Effect of particle size on modulating turbulent intensity. International Journal of Multiphase Flow. 1989;15:279–85. DOI:10.1016/0301-9322(89)90076-1.

[44] Hetsroni G. Particles-turbulence interaction. International Journal of Multiphase Flow. 1989;15:735–46. DOI:10.1016/0301-9322(89)90037-2.

[45] Hadinoto K, Jones EN, Yurteri C, Curtis JS. Reynolds number dependence of gas-phase turbulence in gas-particle flows. International Journal of Multiphase Flow. 2005;31:416–34. DOI:10.1016/j.ijmultiphaseflow.2004.11.009.

[46] Ferrante A, Elghobashi S. On the physical mechanisms of two-way coupling in particle-laden isotropic turbulence. Physics of Fluids. 2003;15: 315–29. DOI:10.1063/1.1532731.

[47] Van den Berg TH, Luther S, Lohse D. Energy spectra in microbubbly turbulence. Physics of Fluids. 2006;18: 1–4. DOI:10.1063/1.2185688.

[48] Mazzitelli IM, Lohse D, Toschi F. The effect of microbubbles on developed turbulence. Physics of Fluids. 2003;15:L5–8. DOI:10.1063/1.1528619.

[49] Rensen J, Luther S, Lohse D. The effect of bubbles on developed turbulence. Journal of Fluid Mechanics. 2005;538:153–87. DOI:10.1017/S0022112005005276.

[50] Elghobashi SE, Truesdell GC. On the two-way interaction between homogeneous turbulence and dispersed solid particles. 1: Turbulence modification. Physics of Fluids. 1993;5: 1790–801.

[51] Nielsen DR, Daugulis AJ, McLellan PJ. A novel method of simulating oxygen mass transfer in two-phase partitioning bioreactors. Biotechnology and Bioengineering. 2003;83:735–42. DOI:10.1002/bit.10721.

[52] Versteeg HK, Malalasekera W. An introduction to computational fluid dynamics: the finite volume method. 2nd ed. Essex, England: Pearson Education; .

[53] Joshi JB, Nere NK, Rane C V, Murthy BN, Mathpati CS, Patwardhan AW, Ranade V V. CFD simulation of stirred tanks: Comparison of turbulence models. Part I: Radial flow impellers. Canadian Journal of Chemical Engineering. 2011;89:23–82. DOI: 10.1002/cjce.20446.

[54] Lane GL. Computational modelling of gas-liquid flow in stirred tanks [PhD thesis]. The University of Newcastle, Australia, 2006.

[55] Elghobashi S. Particle-laden turbulent flows: direct simulation and closure models. Applied Scientific Research. 1991;48:301–14. DOI:10.1007/BF02008202.

[56] Lathouwers D. Modelling and simulation of turbulent bubbly flow [PhD thesis]. Delft University of Technology, The Netherlands, 1999.

[57] ANSYS Academic Research Mechanical and CFD, Release 17.2, Theory Guide 2016.

[58] Lane GL, Schwarz MP, Evans GM. Modelling of the interaction between gas and liquid in stirred vessels. In: 10th European Conference on Mixing; 2000; Delft, The Netherlands: p. 197–204.

[59] Scargiali F, D'Orazio A, Grisafi F, Brucato A. Modelling and simulation of gas–liquid hydrodynamics in mechanically stirred tanks. Chemical Engineering Research and Design. 2007; 85:637–46. DOI:10.1205/CHERD06243.

[60] Zhang D, Deen NG, Kuipers JAM. Numerical simulation of the dynamic flow behavior in a bubble column: A study of closures for turbulence and interface forces. Chemical Engineering Science. 2006;61:7593–608. DOI: 10.1016/j.ces.2006.08.053.

[61] Ishii M, Zuber N. Drag coefficient and relative velocity in bubbly, droplet or particulate flows. AIChE Journal. 1979;25:843–55. DOI:10.1002/aic.690250513.

[62] Behzadi A, Issa RI, Rusche H. Modelling of dispersed bubble and droplet flow at high phase fractions. Chemical Engineering Science. 2004;59: 759–70. DOI:10.1016/j.ces.2003.11.018.

[63] Simonnet M, Gentric C, Olmos E, Midoux N. Experimental determination of the drag coefficient in a swarm of

bubbles. Chemical Engineering Science. 2007;62:858–66. DOI:10.1016/j.ces.2006.10.012.

[64] Baltussen MW, Seelen LJH, Kuipers JAM, Deen NG. Direct numerical simulations of gas-liquid-solid. Chemical Engineering Science. 2013;100:293–9. DOI:10.1016/j.ces.2013.02.052.

[65] Baltussen MW, Kuipers JAM, Deen NG. Direct numerical simulation of effective drag in dense gas-liquid-solid three-phase flows. Chemical Engineering Science. 2017;158:561–8. DOI:10.1016/j.ces.2016.11.013.

[66] Vaidheeswaran A, Hibiki T. Bubble-induced turbulence modeling for vertical bubbly flows. International Journal of Heat and Mass Transfer. 2017;115:741–52. DOI:10.1016/j.ijheatmasstransfer.2017.08.075.

[67] Magolan BL. Extending bubble-induced turbulence modeling applicability in CFD through incorporation of DNS understanding [PhD thesis]. Massachusetts Institute of Technology, United States of America, 2018.

[68] Colombo M, Fairweather M. Multiphase turbulence in bubbly flows: RANS simulations. International Journal of Multiphase Flow. 2015;77:222–43. DOI:10.1016/j.ijmultiphaseflow.2015.09.003.

[69] Rzehak R, Krepper E. CFD modeling of bubble-induced turbulence. International Journal of Multiphase Flow. 2013;55:138–55. DOI:10.1016/j.ijmultiphaseflow.2013.04.007.

[70] Mandø M, Lightstone MF, Rosendahl L, Yin C, Sørensen H. Turbulence modulation in dilute particle-laden flow. International Journal of Heat and Fluid Flow. 2009;30:331–8. DOI:10.1016/j.ijheatfluidflow.2008.12.005.

[71] Horender S, Hardalupas Y. Fluid-particle correlated motion and turbulent energy transfer in a two-dimensional particle-laden shear flow. Chemical Engineering Science. 2010;65:5075–91. DOI:10.1016/j.ces.2010.05.033.

[72] Rols JL, Condoret JS, Fonade C, Goma G. Mechanism of enhanced oxygen transfer in fermentation using emulsified oxygen-vectors. Biotechnology and Bioengineering. February 20, 1990;35:427–35. DOI:10.1002/bit.260350410.

[73] Mcmillan JD, Wang DIC. Mechanisms of oxygen transfer enhancement during submerged cultivation in perfluorochemical-in-water dispersions. Annals of the New York Academy of Sciences. 1990;589:283–300. DOI:10.1111/j.1749-6632.1990.tb24253.x.

[74] Lamont J, Scott D. An eddy cell model of mass transfer into the surface of a turbulent liquid. AIChE Journal. 1970;16:513–9. DOI:10.1002/aic.690160403.

[75] Shabalala NZP, Harris M, Leal Filho LS, Deglon DA. Effect of slurry rheology on gas dispersion in a pilot-scale mechanical flotation cell. Minerals Engineering. 2011;24:1448–53. DOI:10.1016/j.mineng.2011.07.004.

[76] Bakker CW, Meyer CJ, Deglon DA. Numerical modelling of non-Newtonian slurry in a mechanical flotation cell. Minerals Engineering. 2009;22:944–50. DOI:10.1016/j.mineng.2009.03.016.

[77] Kataoka I, Besnard DC, Serizawa A. Basic equation of turbulence and modeling of interfacial transfer terms in gas-liquid two-phase flow. Chemical Engineering Communications. November 1, 1992;118:221–36. DOI:10.1080/00986449208936095.

[78] Viollet PL, Simonin O. Modelling dispersed two-phase flows: closure,

validation and software development. Appl Mech Rev. June 1, 1994;47:80–4. DOI:10.1115/1.3124445.

[79] Mudde RF, Simonin O. Two- and three-dimensional simulations of a bubble plume using a two-fluid model. Chemical Engineering Science. November 1, 1999;54:5061–9. DOI: 10.1016/S0009-2509(99)00234-1.

[80] Bel F'dhila R, Simonin O. Eulerian prediction of a turbulent bubbly flow downstream of a sudden pipe expansion. In: 6th Workshop on Two-Phase Flow Predictions; 1992; Erlangen, Germany: p. 264–73.

[81] Abufalgha AA, Clarke KG, Pott RWM. Characterisation of bubble diameter and gas hold-up in simulated hydrocarbon-based bioprocesses in a bubble column reactor. Biochemical Engineering Journal. 2020;158. DOI: 10.1016/j.bej.2020.107577.

[82] Abufalgha AA, Pott RWM, Cloete JC, Clarke KG. Gas–liquid interfacial area and its influence on oxygen transfer coefficients in a simulated hydrocarbon bioprocess in a bubble column reactor. Journal of Chemical Technology and Biotechnology. 2021;96:1096–106. DOI: 10.1002/jctb.6625.